Supplement of Biogeosciences, 18, 831–847, 2021
https://doi.org/10.5194/bg-18-831-2021-supplement

Biogeosciences Open Access EGU

Supplement of

Patterns of plant rehydration and growth following pulses of soil moisture availability

Andrew F. Feldman et al.

Correspondence to: Andrew F. Feldman (afeld24@mit.edu)

S1. Pulse Growth Detection

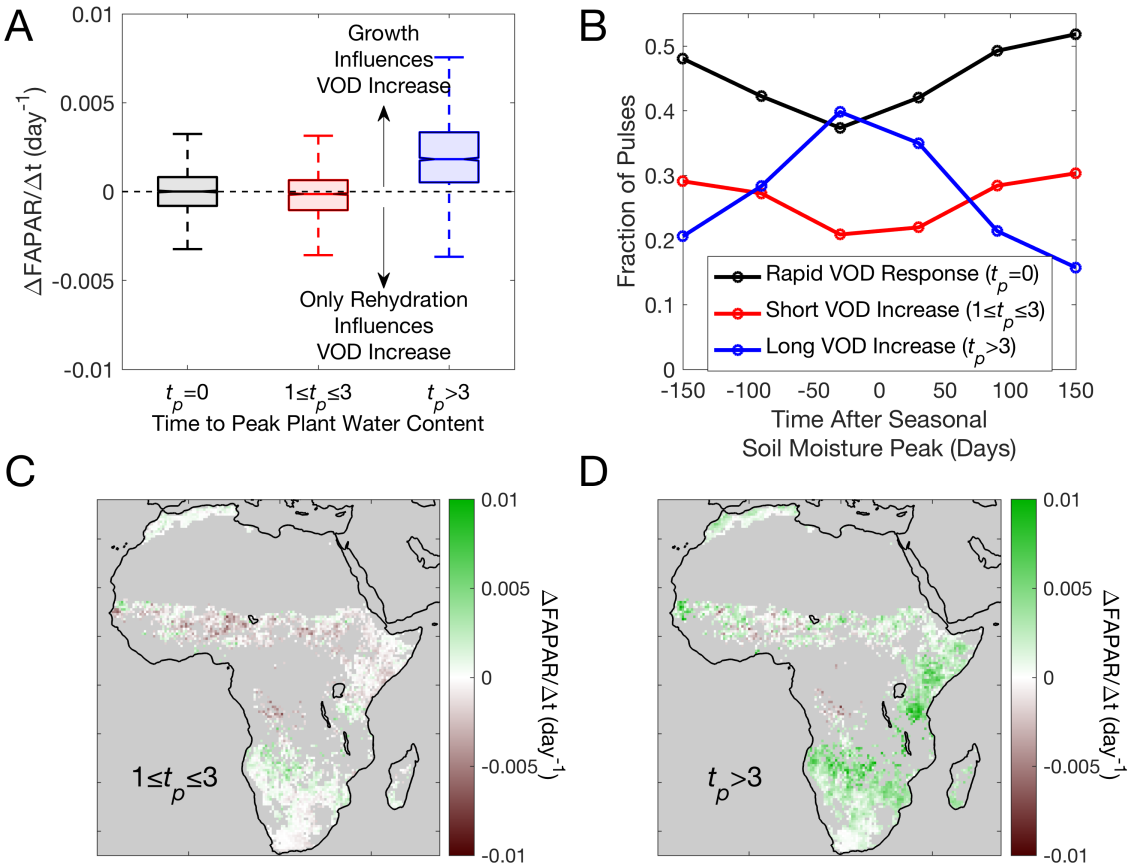

Fig. S1. Same as Fig. 5, but using fraction of absorbed photosynthetically active radiation which is derived from different measurement frequencies than LAI.

S2. VOD Increase Frequency Before Drydown

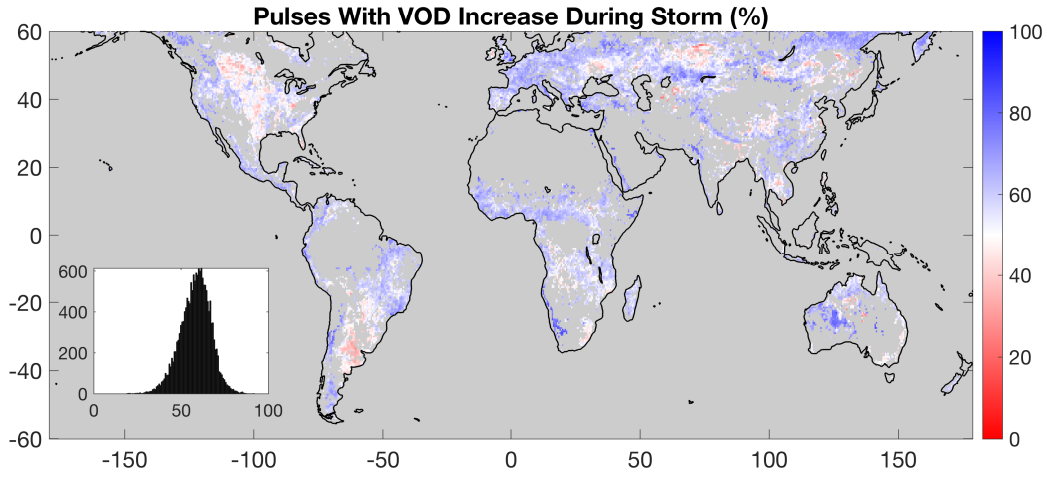

Fig. S2. Percentage of pulses where VOD increases before the drydown initiation (during the storm). Only regions with median t_p of zero are shown. The inset shows the spatial histogram of

the metric. 83% of the regions typically show increases in VOD coincident with soil moisture increases (during the storm before the drydown).

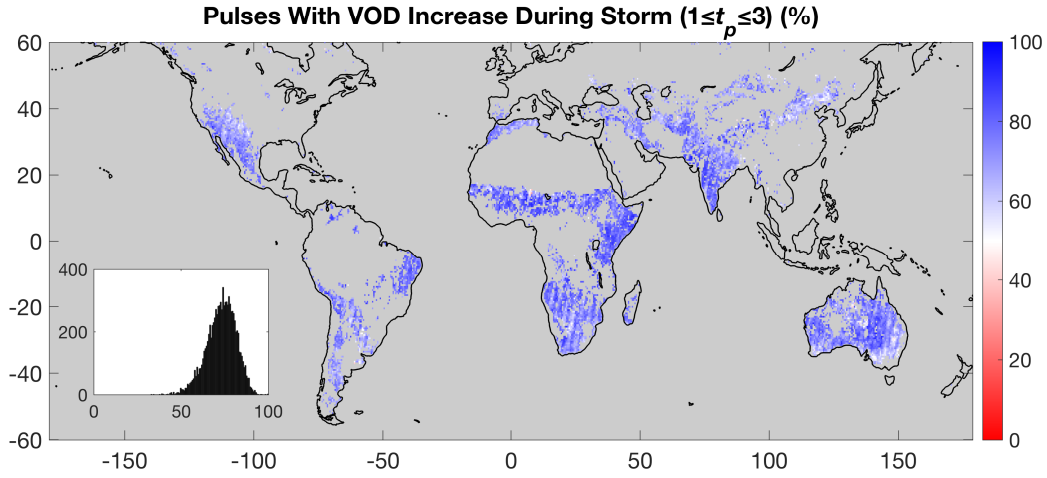

Fig. S3. Percentage of pulses with $1 \leq t_p \leq 3$ where VOD increases before the drydown initiation (during the storm). Only regions with median $t_p \geq 1$ are shown. The inset shows the spatial histogram of the metric.

S2. t_p Estimation Uncertainty

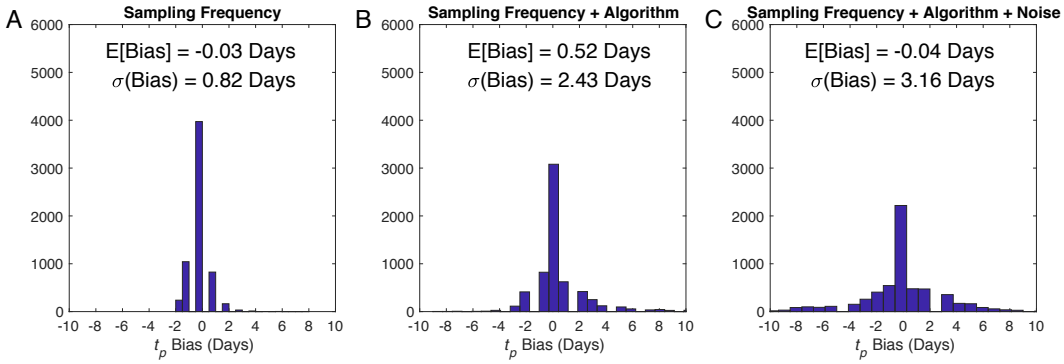

Fig. S4. Simulation with expected behavior of VOD during drying as found in (Feldman et al., 2018). True t_p magnitudes vary randomly. (A) t_p biases due to effects of SMAP's 2-3 day rather than daily sampling frequency. (B) Same as (A) with additional effect of the MT-DCA estimation procedure on t_p. (C) Same as (B) with additional effect of random noise on the order expected from the satellite microwave instrument.

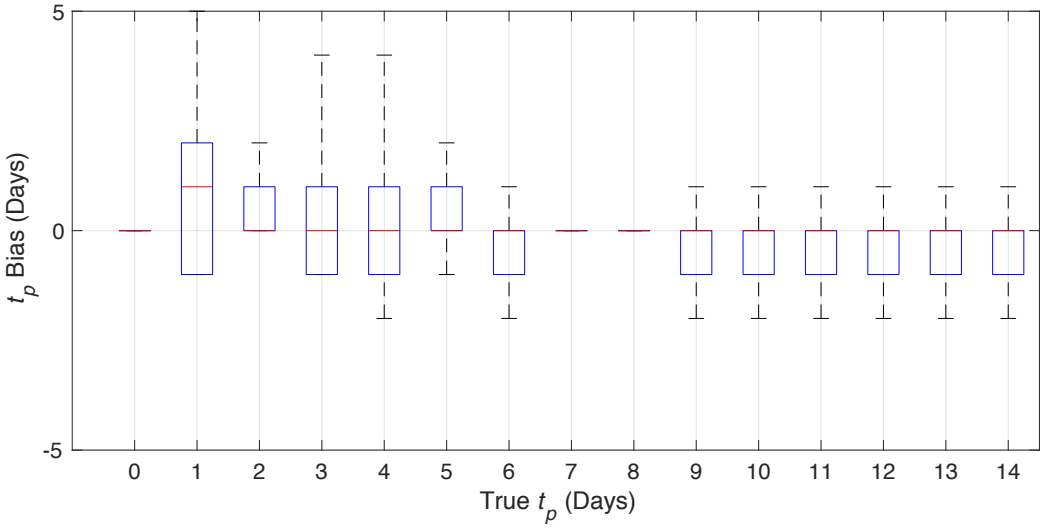

Fig. S5. Effects of SMAP's irregular (1-3-day) sampling frequency on t_p estimates binned as a function of true t_p. The Nyquist frequency for SMAP is approximately 0.2 per day (5-day period). This results in larger variance of t_p estimates when true t_p is less than the Nyquist period.

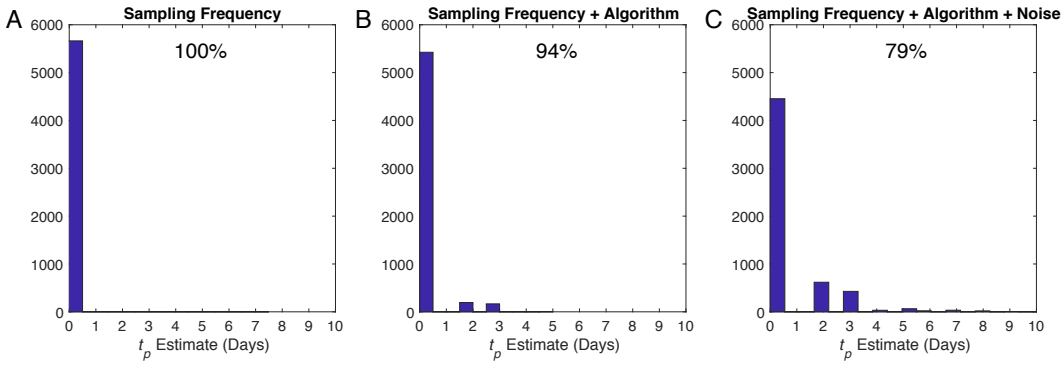

Fig. S6. Simulated detection of whether t_p is zero or non-zero. Randomly generated series all had true t_p of zero. (A) Test indicates SMAP 2-3 day sampling frequency does not hinder detection of t_p of zero. There were no false detections of t_p greater than zero. (B) The use of the MT-DCA algorithm had few false detections of t_p greater than zero when true t_p is zero. (C) Incorporating random noise into the algorithm appears to increase false detection of non-zero t_p the most. Ultimately, all effects together still result in frequent correct detection of true t_p of zero.

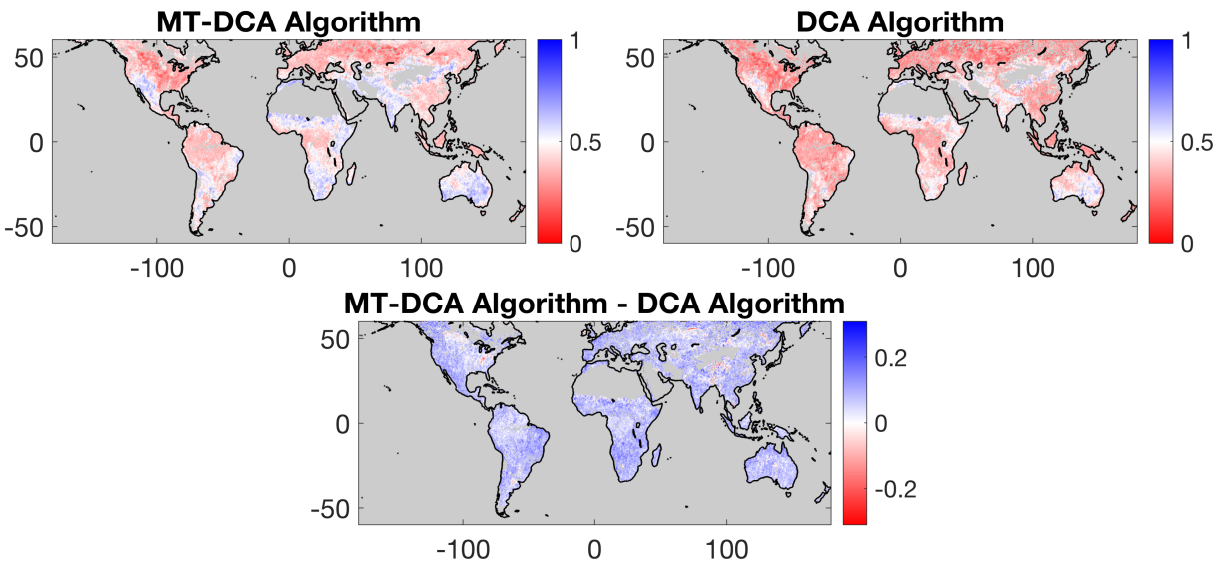

Fig. S7. Non-zero t_p occurrences may be artificially reduced due to algorithmic noise in the DCA algorithm and it is mitigated in the MT-DCA algorithm used here. Probability of $t_p \geq 1$ day using (A) MT-DCA algorithm used here and (B) DCA algorithm. (C) Difference in A and B or the change in probability of occurrence of non-zero t_p using the MT-DCA algorithm instead of the DCA algorithm.

S3. Soil-Plant-Atmosphere Model

S3.1 Plant Components

To investigate the underlying mechanisms that alter plant rehydration timescales, we evaluate plant hydraulic storage timescales under varying conditions after a surface soil moisture pulse using a plant hydraulic model. We specifically choose a one-dimensional SPAC model, assessed in previous studies (Carlson and Lynn, 1991; Hartzell et al., 2017; Lhomme et al., 2001; Zhuang et al., 2014). This model uses governing equations based on the cohesion-tension theory of water potential-driven vertical flow from soil to atmosphere, but has fewer discretized soil and plant components than more complex SPAC model formulations (Mackay et al., 2015; Sperry et al., 2016, 1998). This relative simplicity is advantageous because of its reduced number of parameters. The SPAC model formulation explicitly represents root-zone soil, root, xylem, and leaf components, and accounts for plant storage. It is a balance between incoming sap flow and transpiration losses in the xylem in terms of water potential:

$$C\frac{d\psi_w}{dt} = \frac{\psi_x - \psi_w}{R_w} = \frac{\psi_s - \psi_x}{R_x + R_r} - \frac{\psi_x - \psi_L}{R_x} \quad \text{(S1)}$$

$$\psi_x = \frac{\frac{\psi_w}{R_w} + \frac{\psi_S}{(R_r + R_x)} + \frac{\psi_L}{R_x}}{\frac{1}{R_w} + \frac{1}{(R_r + R_x)} + \frac{1}{R_x}} \quad \text{(S2)}$$

where ψ is water potential, R is resistance, and C is capacitance. x, w, s, r, and L subscripts represent xylem, plant-storage, root zone soil, root (soil interface and radial), and leaf components, respectively. The components are shown in Fig. S8. R_x and R_r are set equal due to lack of field parameterizations and each are referred to as plant resistance (R_P) in our simulations. This simplification precludes finer analysis of individual effects of xylem embolism and root-soil interface resistances, but provides a framework to analyze of how whole-plant

resistances influence hydraulic timescales. R_w is allowed to decrease with reductions in ψ_w (Carlson and Lynn, 1991):

$$R_w = R_{w0} RWC^{-1/4} \quad \text{(S3)}$$

R_{w0} is the storage resistance at full capacity when RWC is 1 and is set equal to R_x (or R_P) here due to lack of field information. Relative water content (RWC) is estimated as linearly related to ψ_w:

$$RWC = \frac{-(\psi_w - \psi_{Crit})}{\psi_{Crit}} \quad \text{(S4)}$$

This requires an assumption of a lower limit (ψ_{Crit}) placed on ψ_w. ψ_{Crit} is chosen to be -10 MPa with alterations to this value having little impact on results.

Transpiration is computed based on a mass transfer model:

$$T = \frac{\varepsilon \rho_{air}}{p \rho_w} \frac{VPD}{(R_a + R_s)} \quad \text{(S5)}$$

Vapor pressure deficit (VPD) reaches zero by predawn and a maximum at midday which is a variable drawn within the SPAC simulations. ε is the ratio of dry air and vapor gas constants, or 0.622. The surface pressure (p), water density (ρ_w), and air density (ρ_{air}) are taken to be 100 kPa, 1,000 kg/m^3, and 1.2 kg/m^3. R_s is computed based on the Medlyn stomatal conductance model and is scaled to a canopy scale parameter by normalizing by LAI (Medlyn et al., 2011):

$$R_s = \frac{1}{g_0 + 1.6\left(1 + \frac{g_1}{\sqrt{VPD}}\right)\frac{A}{C_a}} \left(\frac{1}{LAI}\right) \quad \text{(S6)}$$

where g_0 and g_1 are model parameters assuming savanna values to be -0.007 mol m^{-2} s^{-1} and 6 kPa$^{1/2}$, respectively. Ambient CO_2 concentration (C_a) is assumed constant at 400 μmol/mol. Net assimilation rate (A) is decreased from 6 to 4 μmol m^{-2} s^{-1} over the duration of drying (Xu and Li, 2006). The aerodynamic resistance of turbulent, vertical transport of vapor is computed based on neutral conditions (no surface-air temperature gradient):

$$R_a = \frac{1}{\kappa^2 v} ln\left(\frac{z-d}{z_0}\right)^2 \quad \text{(S7)}$$

The wind speed (v) is held constant for a height of 2 m (z) and is variable based on drawn values within the simulations. The vegetation height is taken to be 0.5 m (for shrubs and grasses) and as such the estimated roughness height (z_0) is 0.05 m and estimated zero plane displacement (d) is 0.375 m. The von Karman constant, κ, is 0.41.

S3.2 Soil Component - Infiltration

Moisture pulse infiltration to the root zone is additionally assessed. We compute ψ_S at each 5 cm layer from 0 to 1 m by numerically solving the soil water balance with Richard's equation to determine the time of unsaturated flow from the rain-wetted surface soil layer to the root zone:

$$\frac{\partial \theta}{\partial t} = \frac{\partial}{\partial z}\left[K(\theta)\left[\frac{d\psi_s}{d\theta}\frac{\partial \theta}{\partial z} + 1\right]\right] \quad \text{(S8)}$$

where θ is soil moisture and K is unsaturated hydraulic conductivity. Note that Eq. S8 takes the same form as Eq. S1 (with Ohm's law analogy) with a potential gradient from surface to root zone, the inverse of K serving as soil resistance, and integral of soil layer depth representing soil storage capacitance. Soil retention curves are used to define the relationship between root zone soil moisture (θ) and potential (ψ_s) as well as soil hydraulic conductivity (K) (Brooks and Corey, 1966):

$$\psi_s(\theta) = \psi_{sat}\left(\frac{\theta}{n}\right)^{-b} \quad \text{(S9)}$$

$$K(\theta) = K_s\left(\frac{\theta}{n}\right)^{c} \quad \text{(S10)}$$

b is the Brooks-Corey parameter which also defines c, or 2b+3. n is porosity. Soil moisture decay is imposed as a boundary condition in the top layer. In semi-arid regions globally, the e-folding decay rate for surface soil moisture is approximately 10 days (McColl et al., 2017). Losses due to plant water uptake, soil evaporation, and percolation are encompassed in this loss rate. Soil moisture is assumed to decay uniformly during the time period instead of slowed decay overnight as in (Daly et al., 2004). After the soil pulse reaches the lower layers, each above layer decays with the boundary condition. All layers below 0.05 m are assumed to decay four times slower than the surface layer due to reduced impacts of soil evaporation (Gebauer et al., 2002). Z defines the layer where ψ_s is coupled to the SPAC model.

Note that the SPAC model does not account for many factors including the effects of osmotic adjustment under drying. However, more complex parametrizations include uncertainties with more parameters, especially those not that well constrained by previous measurements. This exemplifies the importance to bear in mind the multi-dimensional parameter space underlying this model and thus the wide range of scenarios that may influence time variations of plant and soil potentials.

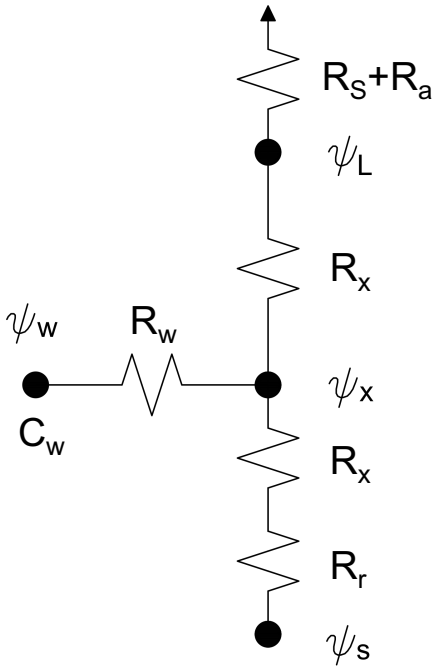

Fig. S8. Soil-Plant-Atmosphere Continuum Model Diagram

S3.3 SPAC Model Simulation General Notes

Using the SPAC model, ψ_W time series are simulated following soil moisture pulses in order to investigate how different factors influence the simulated pulse response timescales. A three-day spin-up period allows the plant and soil water potential components to come to an initial equilibrium. An additional two-day drying period is implemented before the surface moisture pulse. The model is run at a 3 second time step. This 3 second time step and 0.05 m soil layer intervals prohibits model "break down" when solving explicitly. A rain pulse occurs at 6:00 AM after the two-day drying period. The pulse is followed by eight days of drying. t_p is computed as the peak ψ_W following the pulse, analogously to the satellite-observed plant water content. This simulation is repeated using a Monte Carlo approach (n = 1,000), randomly sampling SPAC model parameters from given parameter ranges based on previous field measurements. t_p sensitivity to a given parameter is evaluated by fixing the respective parameter and randomly varying all other parameters ("All" scenario). To evaluate pairwise interactions between sets of two parameters, an additional parameter to that in the "All" scenario is fixed and all other parameters are randomly varied.

The SPAC model parameter space is bounded to common semi-arid meteorological conditions and plant types (Table S1; see also SI for parameter bound justification based on available databases (Kattge et al., 2020) and measurements from the literature). Dryland plants and climatic conditions are chosen for investigation as global drylands primarily are found in this study to exhibit multi-day rehydration (slow rehydration). The SPAC model is used to evaluate the scenarios under which plant-storage water potential timescales exceed a day. The stomatal and plant resistances are linearly decreased over three days to randomly varying degrees (R_P recovery and R_S impairment factors in Table S1) following the soil moisture pulse, common occurrences following rewetting due to drought recovery mechanisms (Martorell et al., 2014; Rodriguez-Dominguez and Brodribb, 2020; West et al., 2007).

S3.4 SPAC Model Parameter Range Justification

S3.4.1 Whole Plant Resistance (R_p) and Its Recovery

We consult the TRY plant trait database and a review article for whole plant conductance values (Kattge et al., 2020; Mencuccini, 2003). Across species the whole plant conductance distribution is approximately lognormally distributed. We convert to plant resistance (normalized on a per leaf basis) with approximate 5th, 50th, and 95th percentiles of $5x10^6$ MPa s/m, $3x10^7$ MPa s/m, $1x10^8$ MPa s/m respectively. While this is across species, dryland grass species are comparable to this distribution at approximately $2x10^7$ MPa s/m (Carlson and Lynn, 1991; Hunt and Nobel, 1987). Further, R_p can increase by up to a factor of ten from nominal to dry conditions (Brodribb and Cochard, 2009; Rodriguez-Dominguez and Brodribb, 2020; Trifilò et al., 2004; Zarebanadkouki and Carminati, 2014). Therefore, we set the R_p range between $1x10^6$ MPa s/m and $1x10^9$ MPa s/m.

If the plant is dried for a period, R_p increases. Upon rewetting, R_p can take two to four days to recover and decrease by a factor of five along an approximately linear trend in time (Lo Gullo et al., 1998; North and Nobel, 1995). We therefore allow R_p to decrease by a factor of one to ten linearly for approximately three days. Given the lower confidence of this R_p factor of recovery measure, we allow it to decrease by up to a factor of ten.

S3.4.2 Rooting Profile Depth

We consult the TRY plant trait database and find roots to typically located within the first meter of soil (Kattge et al., 2020). In general, semi-arid grasses tend to have most roots located between 0.1 m and 0.6 m below the surface while shrub rooting profiles are between 0.3 m and 0.7 m below the surface (Reynolds et al., 2004). We therefore allow rooting profiles to vary between 0.1 and 1 meters.

S3.4.3 Capacitance

Semi-arid grass and shrub species have capacitance values that range between $1x10^{-6}$ m/MPa and $1x10^{-4}$ m/MPa (Carlson and Lynn, 1991; Hunt and Nobel, 1987; Hunt Jr et al., 1991; Nobel and Jordan, 1983). Succulent and tree species tend to have values above $1x10^{-3}$ m/MPa (Carlson and Lynn, 1991; Meinzer et al., 2003; Scholz et al., 2007), and we do not anticipate these plant functional types will dominate the satellite view. Therefore, we constrain capacitance values between $1x10^{-6}$ m/MPa and $1x10^{-4}$ m/MPa. Values are normalized on a unit area basis. Please note that these ranges are formulated from a scarce number of available measurements (Scholz et al., 2011).

S3.4.4 Stomatal Resistance Impairment Factor

We allow for stomatal resistance to decrease by up to a factor of 10. Previous measurements show stomatal conductance increases on this order over a few days following rewetting (Blackman et al., 2009; Brodribb and Cochard, 2009; Chen et al., 2010; Fereres et al., 1979; Martorell et al., 2014).

S3.4.5 Soil Water Potential Values

Soil water potential values can range greatly in arid to semi-arid regions. Dry soil conditions can create surface and rootzone water potential values commonly down to -5 MPa (Golluscio et al., 1998; Montaña et al., 1995). While the rootzone can become much drier, we

choose -5 MPa as our lower bound on initial soil water potential as this provides a range of soil water potentials that can delay the infiltration front on the order of minutes to days. -0.5 MPa is selected as the upper bound of initial soil water potential as a dry soil value that may not create infiltration delays, but may create higher root resistances. Furthermore, we allow the moisture pulse to increase soil water potential at least up to -0.3 MPa as it is above the wettest initial soil water potential value, but still considered a small pulse that may not reach lower soil layers of the rootzone. The upper bound of the soil water potentials is allowed to approach zero or -0.001 for the greatest rewetting events.

S3.4.6 VPD and Wind Speed

We consult a range of values exhibited for drylands under nominal conditions from reanalysis data (GMAO, 2015). Typical values of VPD after rewetting range from 1 to 5 kPa while wind speeds reach typically up to 8 m/s (Feldman et al., 2019).

Table S1. SPAC model simulation parameters. Each parameter is drawn from a uniform distribution with chosen "Lower" and "Upper" bounds shown. "Low" and "High" scenario columns represent the value a parameter is held fixed at for repeated simulations under the respective scenario. See the SI for references for parameter bounds.

SPAC Model Simulation Parameters	Lower Bound	"Low" Scenario	"High" Scenario	Upper Bound
Rooting Profile Depth Mean (m)	0.1	0.3	0.7	1
Plant Resistance (R_P) (MPa/(m/s))	1.E+06	5.E+06	5.E+08	1.E+09
Capacitance (C) (m/MPa)	1.E-06	1.E-06	1.E-04	1.E-04
Vapor Pressure Deficit (VPD) (kPa)	1	2	5	5
Wind Speed (m/s)	1	2	7	8
Stomatal Resistance Impairment Factor	-10	-10	-1	-1
Plant Resistance (R_P) Linear Recovery Factor	1	1	10	10
Pulsed Surface Soil Water Potential (MPa)	-0.5	-0.3	-0.01	-0.001
Initial Soil Water Potential (MPa)	-5	-5	-0.5	-0.5

S3.5 SPAC Model Simulation Results

High initial plant resistance that decreases over multiple days are the sufficient conditions for multi-day ψ_w increases to occur upon soil rewetting (Figs. S9 to S12). This means that multi-day plant rehydration does not occur unless plant resistance is initially high (Fig. S9A; $R_P \geq 10^7$ MPa/(m/s)). Similarly, multi-day plant rehydration does not occur unless plant resistance decreases (Fig. S9B; R_P recovery factor >1). Increasing capacitance up to values common for shrub species increases the likelihood for multi-day ψ_w increases, but cannot solely cause slow rehydration within this range of parameters (Fig. S9 "High C" cases and Fig. S10A). Even though rehydration is faster if stomatal conductance increases in time, an expected scenario in these cases (Rodriguez-Dominguez and Brodribb, 2020), multi-day rehydration can still occur (Fig. S9 "large R_S impairment" cases and Fig. S10B). Environmental factors such as wind speed and VPD which influence transpiration as well as rooting depth do not influence multi-day rehydration occurrences, at least in these scenarios (Figs. S9 and S10). It is important to note that these aforementioned conditions that lead to multi-day plant rehydration do not consider soil resistance limitations (slow infiltration is dealt with separately). In these scenarios, the soil is

initially only moderately dry and the pulse reaches the rootzone in the same day as the pulse. However, dry soils accompany high root resistances, for instance, and drier soils precede 1-3-day VOD increases observed in this study (Fig. 7A).

We further investigate effects of soil conductance on plant rehydration timescales by additionally varying pulse magnitude and initial soil moisture within our SPAC model simulations. Slow plant rehydration occurs if at least two of the three conditions occur: dry initial rootzone soil moisture, small rewetting pulses, and deeper roots (Figs. S11 and S12). Each one of these conditions alone is insufficient to slow plant rehydration (for example, deeper roots alone do not cause slow plant rehydration as seen in Figs. S11 and S12C). These conditions all promote a slow infiltration front due to initially high soil resistance that decreases over time - analogously to initially high and decreasing R_p in the plant limitation cases (Fig. S11). These scenarios isolate slow plant rehydration due only to soil resistance by preventing additional limitations due to plant resistances. This is at least possible in this SPAC model where plant and soil resistances can be uncoupled. Multi-day plant rehydration occurs more frequently with an initially drier rootzone, smaller pulses, and deeper rooting profiles (Figs. S11 and S12). However, under interacting conditions, the moisture pulse will not reach the rootzone altogether, given the assumptions of homogenous soil and concentrated rootzone. Reductions in cases of multi-day plant rehydration occur for this reason at extremes of drier initial soils, smaller pulses, and deeper roots (as seen in Figs. S11 and S12). Nevertheless, for shallow rooting profiles, the infiltration front will still reach the rootzone, albeit slowly, under very dry initial soil conditions and small pulses (Fig. S11B).

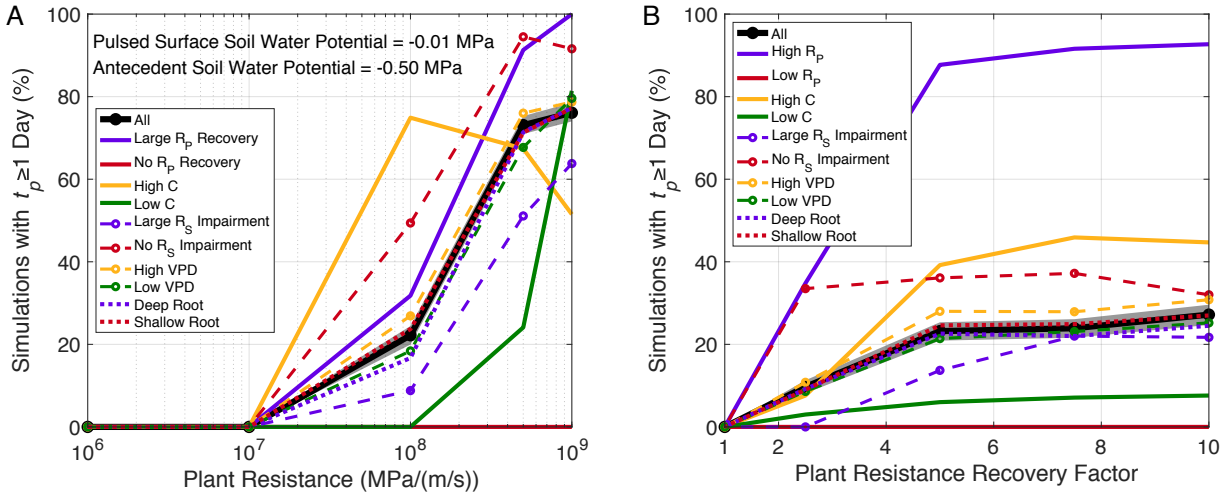

Fig. S9. The percentage of simulations with a ψ_W peak occurring over one day after a soil moisture pulse, using repeated simulations with the SPAC model. (A) Plant resistance is held fixed at each respective value on the x-axis. (B) Plant resistance recovery factor (factor by which R_P decreases over three days) is held fixed at each respective value on the x-axis. The remaining variables are drawn from uniform distributions in Table S1 for 1,000 iterations in the "All" scenario. All other lines are generated the same as "All," but fix one additional parameter (noted in the legend) to evaluate pairwise interactions. Grey shading provides the 5th and 95th percentile of the multi-day rehydration occurrence variability in "All" scenarios using bootstrapping. The "low" and "high" values used to fix parameters are shown in Table S1. High and low wind scenarios are similar to "All" scenario and are not shown.

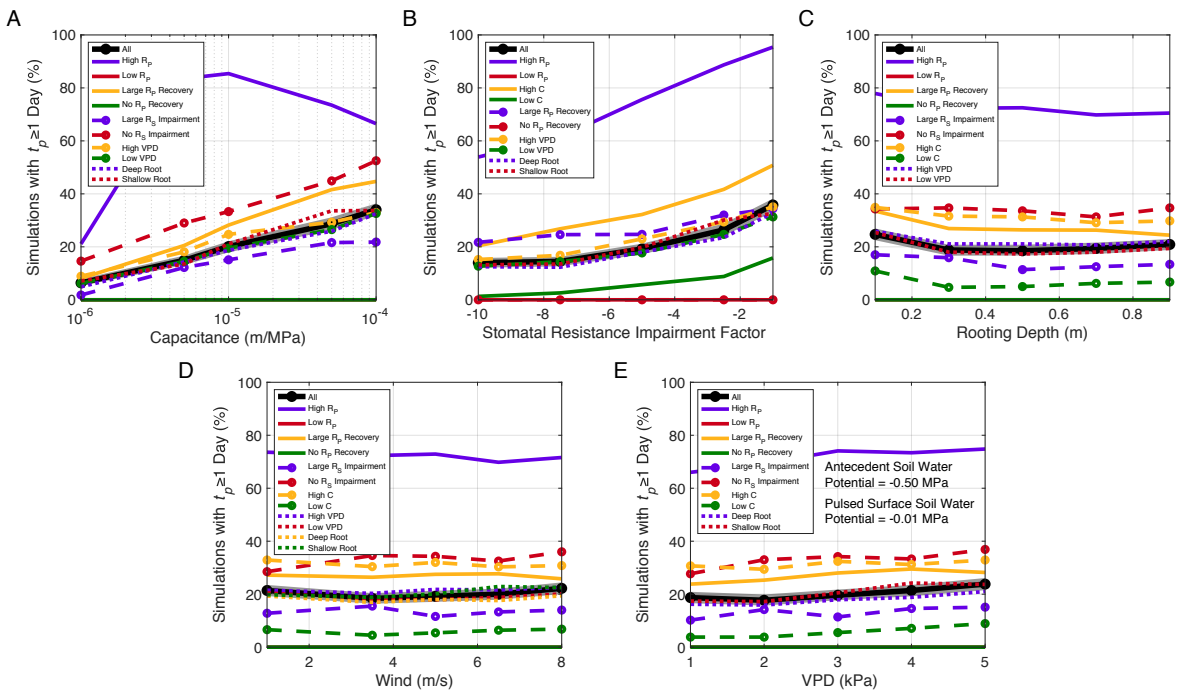

Fig. S10. Same as Fig. S9, but fixing capacitance (A), R_S impairment factor (B), rooting depth (C), wind (D), and VPD (E). High and low wind scenarios are similar to "All" scenario and are not shown.

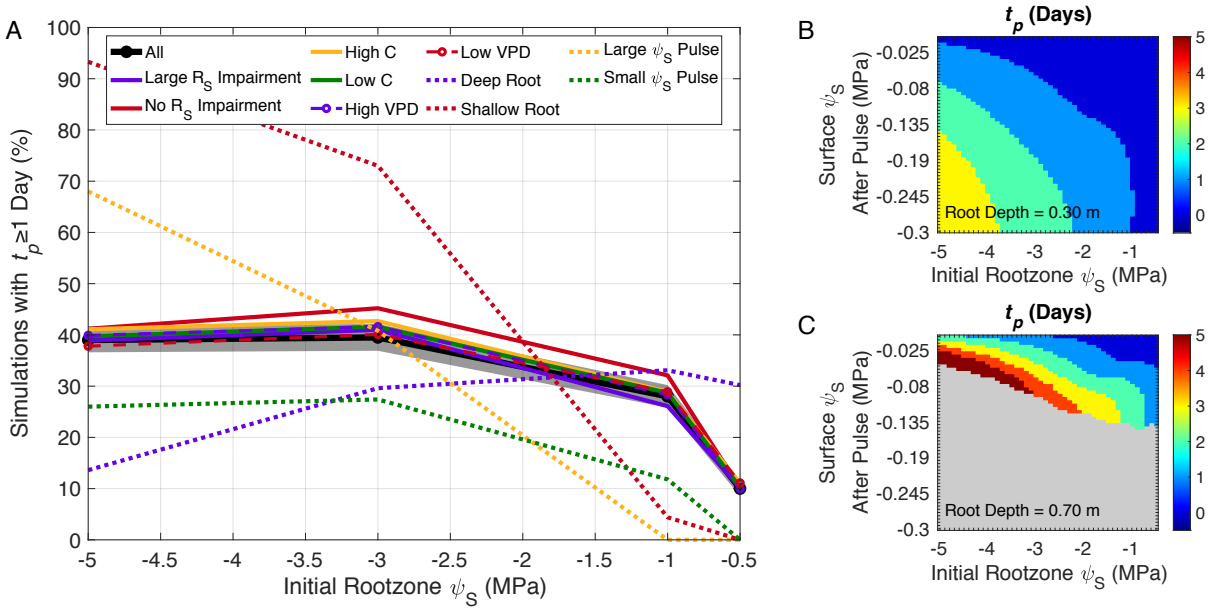

Fig. S11. (A) Same as Figs. S9 and S10, but includes variations of initial and pulsed ψ_S conditions. Also, $R_P = 10^7$ MPa/(m/s) and does not decrease which isolates only soil conditions that would cause multi-day ψ_W rehydration. ψ_W peak timing for rooting depth of (B) 0.3 m and (C) 0.7 m (C = 10^{-6} m/MPa, Wind = 5 m/s, VPD = 3 kPa, no change in R_P or R_S). Grey shading in (C) indicates that the pulse did not impact ψ_W because the pulse did not reach the rootzone. High and low wind scenarios are similar to "All" scenario and are not shown.

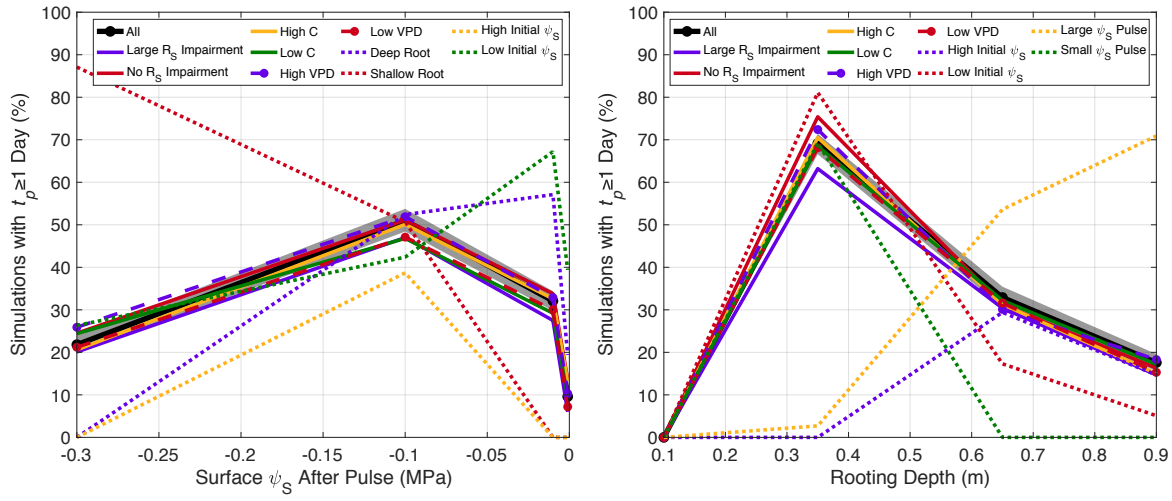

Fig. S12. Same as Figs. S11 where soil conditions are varied, but fixing pulsed ψ_S conditions (A), and rooting depth (B). High and low wind scenarios are similar to "All" scenario and are not shown.

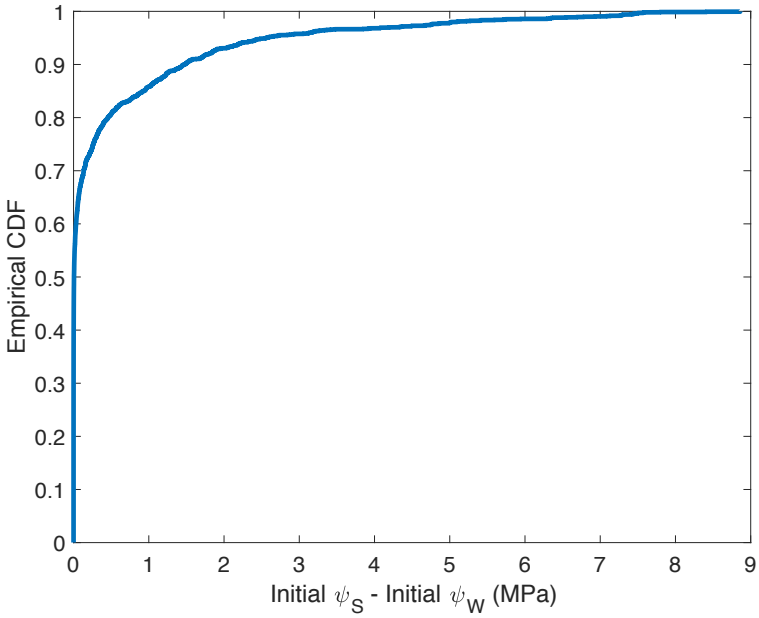

Fig. S13. Cumulative distribution function of degree of pre-dawn equilibration between soil and plant water potentials before the beginning of the storm.

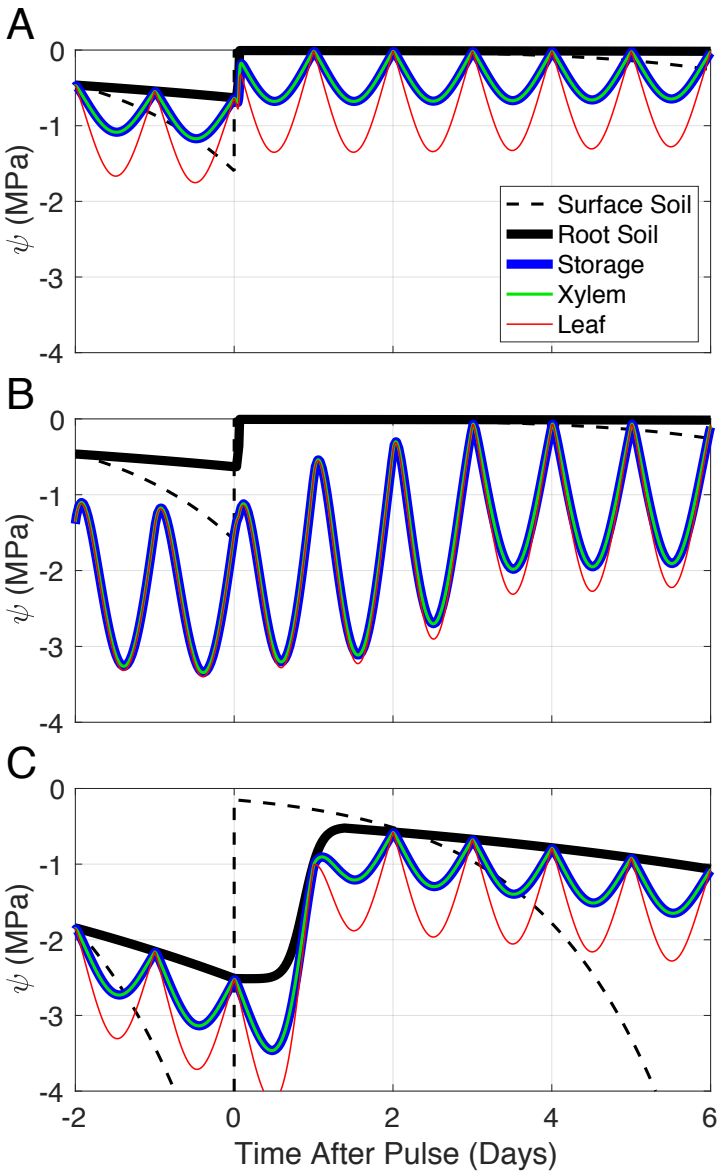

Fig. S14. SPAC model scenarios. Rainfall occurs at 6:00 on Day 0 after a drying period. A: Nominal conditions with C_w of $2x10^{-5}$ m/MPa, R_P of $2x10^7$ MPa/(m/s), root zone concentrated at 0.3 m, and initial soil moisture pulsed from -0.6 MPa to -0.01 MPa. B: Initially higher plant resistance ($R_P = 5x10^8$ MPa/(m/s)) with linear recovery to nominal conditions ($R_P = 5x10^7$ MPa/(m/s)) over three days after pulse. C: Drier initial root zone (surface ψ_S = -2.5 MPa) and smaller pulse conditions (surface ψ_S = -0.15 MPa).

References

Blackman, C.J., Brodribb, T.J., Jordan, G.J., 2009. Leaf hydraulics and drought stress: Response, recovery and survivorship in four woody temperate plant species. Plant, Cell Environ. 32, 1584–1595. https://doi.org/10.1111/j.1365-3040.2009.02023.x

Brodribb, T.J., Cochard, H., 2009. Hydraulic failure defines the recovery and point of death in water-stressed conifers. Plant Physiol. 149, 575–584. https://doi.org/10.1104/pp.108.129783

Brooks, R.H., Corey, A.T., 1966. Properties of Porous Media Affecting Fluid Flow. J. Irrig. Drain. Div. 92, 61–90.

Carlson, T.N., Lynn, B., 1991. The effects of plant water storage on transpiration and radiometric surface temperature. Agric. For. Meteorol. 57, 171–186. https://doi.org/10.1016/0168-1923(91)90085-5

Chen, J.W., Zhang, Q., Li, X.S., Cao, K.F., 2010. Gas exchange and hydraulics in seedlings of Hevea brasiliensis during water stress and recovery. Tree Physiol. 30, 876–885. https://doi.org/10.1093/treephys/tpq043

Daly, E., Porporato, A., Rodríguez-Iturbe, I., 2004. Coupled Dynamics of Photosynthesis, Transpiration, and Soil Water Balance. Part I: Upscaling from Hourly to Daily Level. J. Hydrometeorol. 5, 546–558. https://doi.org//10.1175/1525-7541(2004)005<0546:CDOPTA>2.0.CO;2

Feldman, A.F., Short Gianotti, D.J., Konings, A.G., McColl, K.A., Akbar, R., Salvucci, G.D., Entekhabi, D., 2018. Moisture pulse-reserve in the soil-plant continuum observed across biomes. Nat. Plants 4, 1026–1033. https://doi.org/10.1038/s41477-018-0304-9

Feldman, A.F., Short Gianotti, D.J., Trigo, I.F., Salvucci, G.D., Entekhabi, D., 2019. Satellite-Based Assessment of Land Surface Energy Partitioning–Soil Moisture Relationships and Effects of Confounding Variables. Water Resour. Res. 55, 10657–10677. https://doi.org/10.1029/2019WR025874

Fereres, E., Cruz-Romero, G., Hoffman, G.J., Rawlins, S.L., 1979. Recovery of Orange Trees Following Severe Water Stress. J. Appl. Ecol. 16, 833. https://doi.org/10.2307/2402857

Gebauer, R.L.E., Schwinning, S., Ehleringer, J.R., 2002. Interspecific Competition and Resource Utilization between Bumblebees. Ecology 83, 2602–2616. https://doi.org/10.2307/3672007

GMAO, 2015. MERRA-2 inst1_2d_asm_Nx: 2d,1-Hourly,Instantaneous,Single-Level,Assimilation,Single-Level Diagnostics V5.12.4, Greenbelt, MD, USA, Goddard Earth Sciences Data and Information Services Center (GES DISC), Accessed: [01.10.19], 10.5067/3Z173KIE2TPD.

Golluscio, R.A., Sala, O.E., Lauenroth, W.K., 1998. Differential use of large summer rainfall events by shrubs and grasses: A manipulative experiment in the Patagonian steppe. Oecologia 115, 17–25. https://doi.org/10.1007/s004420050486

Hartzell, S., Bartlett, M.S., Porporato, A., 2017. The role of plant water storage and hydraulic strategies in relation to soil moisture availability. Plant Soil 503–521. https://doi.org/10.1007/s11104-017-3341-7

Hunt, E.R., Nobel, P.S., 1987. Non-steady-state Water Flow for Three Desert Perennials with Different Capacitances. Aust. J. Plant Physiol. 14, 363–375.

Hunt Jr, E.R., Running, S.W., Federer, C.A., 1991. Extrapolating plant water flow resistances and capacitances to regional scales. Agric. For. Meteorol. 54, 169–195.

Kattge, J., Bönisch, G., Díaz, S., Lavorel, S., Prentice, I.C., Leadley, P., Tautenhahn, S., Werner, G.D.A., .et .al., 2020. TRY plant trait database – enhanced coverage and open access. Glob.

Chang. Biol. 26, 119–188. https://doi.org/10.1111/gcb.14904
Lhomme, J.P., Rocheteau, A., Ourcival, J.M., Rambal, S., 2001. Non-steady-state modelling of water transfer in a Mediterranean evergreen canopy 108, 67–83.
Lo Gullo, M.A., Nardini, A., Salleo, S., Tyree, M.T., 1998. Changes in root hydraulic conductance (K(R)) of Olea oleaster seedlings following drought stress and irrigation. New Phytol. 140, 25–31. https://doi.org/10.1046/j.1469-8137.1998.00258.x
Mackay, D.S., Roberts, D.E., Ewers, B.E., Sperry, J.S., McDowell, N.G., Pockman, W.T., 2015. Interdependence of chronic hydraulic dysfunction and canopy processes can improve integrated models of tree response to drought. Water Resour. Res. 51, 6156–6176. https://doi.org/10.1002/2015WR017200.A
Martorell, S., Diaz-Espejo, A., Medrano, H., Ball, M.C., Choat, B., 2014. Rapid hydraulic recovery in Eucalyptus pauciflora after drought: Linkages between stem hydraulics and leaf gas exchange. Plant, Cell Environ. 37, 617–626. https://doi.org/10.1111/pce.12182
McColl, K.A., Wang, W., Peng, B., Akbar, R., Short Gianotti, D.J., Lu, H., Pan, M., Entekhabi, D., 2017. Global characterization of surface soil moisture drydowns. Geophys. Res. Lett. 44, 3682–3690. https://doi.org/10.1002/2017GL072819
Medlyn, B.E., Duursma, R.A., Eamus, D., Ellsworth, D.S., Prentice, I.C., Barton, C.V.M., Crous, K.Y., De Angelis, P., Freeman, M., Wingate, L., 2011. Reconciling the optimal and empirical approaches to modelling stomatal conductance. Glob. Chang. Biol. 17, 2134–2144. https://doi.org/10.1111/j.1365-2486.2010.02375.x
Meinzer, F.C., James, S.A., Goldstein, G., Woodruff, D., 2003. Whole-tree water transport scales with sapwood capacitance in tropical forest canopy trees. Plant, Cell Environ. 26, 1147–1155. https://doi.org/10.1046/j.1365-3040.2003.01039.x
Mencuccini, M., 2003. The ecological significance of long-distance water transport: Short-term regulation, long-term acclimation and the hydraulic costs of stature across plant life forms. Plant, Cell Environ. 26, 163–182. https://doi.org/10.1046/j.1365-3040.2003.00991.x
Montaña, C., Cavagnaro, B., Briones, O., 1995. Soil water use by co-existing shrubs and grasses in the southern Chihuahuan Desert, Mexico. J. Arid Environ. 31, 1–13. https://doi.org/10.1006/jare.1995.0043
Nobel, P.S., Jordan, P.W., 1983. Transpiration stream of desert species: Resistances and capacitances for a c3, a c4, and a cam plant. J. Exp. Bot. 34, 1379–1391. https://doi.org/10.1093/jxb/34.10.1379
North, G.B., Nobel, P.S., 1995. Hydraulic conductivity of concentric root tissues of Agave deserti Engelm. under wet and drying conditions. New Phytol. 130, 47–57. https://doi.org/10.1111/j.1469-8137.1995.tb01813.x
Ogle, K., Reynolds, J.F., 2004. Plant responses to precipitation in desert ecosystems: Integrating functional types, pulses, thresholds, and delays. Oecologia 141, 282–294. https://doi.org/10.1007/s00442-004-1507-5
Reynolds, J.F., Kemp, P.R., Ogle, K., Fernández, R.J., 2004. Modifying the “pulse-reserve” paradigm for deserts of North America: Precipitation pulses, soil water, and plant responses. Oecologia 141, 194–210. https://doi.org/10.1007/s00442-004-1524-4
Rodriguez-Dominguez, C.M., Brodribb, T.J., 2020. Declining root water transport drives stomatal closure in olive under moderate water stress. New Phytol. 225, 126–134. https://doi.org/10.1111/nph.16177
Scholz, F.G., Bucci, S.J., Goldstein, G., Meinzer, F.C., Franco, A.C., Miralles-Wilhelm, F., 2007. Biophysical properties and functional significance of stem water storage tissues in

Neotropical savanna trees. Plant, Cell Environ. 30, 236–248. https://doi.org/10.1111/j.1365-3040.2006.01623.x

Scholz, F.G., Phillips, N.G., Bucci, S.J., Meinzer, F.C., Goldstein, G., 2011. Size- and Age-Related Changes in Tree Structure and Function, in: Size- and Age-Related Changes in Tree Structure and Function. pp. 341–361. https://doi.org/10.1007/978-94-007-1242-3

Sperry, J.S., Adler, F.R., Campbell, G.S., Comstock, J.P., 1998. Limitation of plant water use by rhizosphere and xylem conductance: Results from a model. Plant, Cell Environ. 21, 347–359. https://doi.org/10.1046/j.1365-3040.1998.00287.x

Sperry, J.S., Wang, Y., Wolfe, B.T., Mackay, D.S., Anderegg, W.R.L., McDowell, N.G., Pockman, W.T., 2016. Pragmatic hydraulic theory predicts stomatal responses to climatic water deficits. New Phytol. 212, 577–589. https://doi.org/10.1111/nph.14059

Trifilò, P., Raimondo, F., Nardini, A., Lo Gullo, M.A., Salleo, S., 2004. Drought resistance of Ailanthus altissima: Root hydraulics and water relations. Tree Physiol. 24, 107–114. https://doi.org/10.1093/treephys/24.1.107

West, A.G., Hultine, K.R., Jackson, T.L., Ehleringer, J.R., 2007. Differential summer water use by Pinus edulis and Juniperus osteosperma reflects contrasting hydraulic characteristics. Tree Physiol. 27, 1711–1720. https://doi.org/10.1093/treephys/27.12.1711

Xu, H., Li, Y., 2006. Water-use strategy of three central Asian desert shrubs and their responses to rain pulse events. Plant Soil 285, 5–17. https://doi.org/10.1007/s11104-005-5108-9

Zarebanadkouki, M., Carminati, A., 2014. Reduced root water uptake after drying and rewetting. J. Plant Nutr. Soil Sci. 177, 227–236. https://doi.org/10.1002/jpln.201300249

Zhuang, J., Yu, G.-R., Nakayama, K., 2014. A Series RCL Circuit Theory for Analyzing Non-Steady-State Water Uptake of Maize Plants. Sci. Rep. https://doi.org/10.1038/srep06720